



Article

Micro Flowers of SrS/Bi₂S₃ Nanocomposite and Its Field Emission Properties

Aarti R. Gunjal¹, Ujjwala P. Chothe¹, Yogesh A. Sethi¹, Rajendra P. Panmand¹,
Jalinder D. Ambekar¹, Milind V. Kulkarni¹, Mahendra A. More² and Bharat B. Kale^{1,*}

¹ Centre for Materials for Electronics Technology (C-MET), Ministry of Electronics and Information Technology (MeitY), Government of India, Panchawati Off Pashan Road, Pune 411008, India; aartitambe22@gmail.com (A.R.G.); k.ujjwala@yahoo.com (U.P.C.); yogeshsethi68@gmail.com (Y.A.S.); rpanmand@gmail.com (R.P.P.); jalindar2009@gmail.com (J.D.A.); milind@cmet.gov.in (M.V.K.)

² Department of Physics, Savitribai Phule Pune University, Pune 411007, India; mam@physics.unipune.ac.in

* Correspondence: bbkale@cmet.gov.in; Tel.: +020-2589-8390

Received: 17 September 2019; Accepted: 26 November 2019; Published: 3 December 2019



Abstract: The three-dimensional hierarchical SrS/Bi₂S₃ heterostructures were synthesized by a template-free single-step hydrothermal method. The structural and morphological studies revealed the formation of a single crystalline orthorhombic heterostructure with rod-like morphologies possessing a high aspect ratio. The field emission properties of SrS/Bi₂S₃ nanorods were investigated. J–E and the Fowler–Nordheim (F–N) plot, as well as long-term field emission (FE) stability, were studied. SrS/Bi₂S₃ nanoflowers have enhanced the FE properties more than the virgin Bi₂S₃. The observed values of the re-producible turn-on field for SrS/Bi₂S₃ defined to draw an emission current density of ca. 1 $\mu\text{A}/\text{cm}^2$ were found to be ca. 2.50 V/ μm , and of the threshold field to draw a current density of ca. 10 $\mu\text{A}/\text{cm}^2$ were found to be ca. 3.00 V/ μm (without visible light illumination). A maximum emission current density of ca. 527 $\mu\text{A}/\text{cm}^2$ was drawn without light and a current density of ca. 1078 $\mu\text{A}/\text{cm}^2$ with light, which is higher than that of pristine Bi₂S₃.

Keywords: field emission; SrS/Bi₂S₃; hydrothermal method

1. Introduction

Nanomaterials have been attracting great attention for catalytic, electronics, and electro-optical applications. Recently, architectural changes in the nanomaterial design and their orientation have attracted scientists because of their potential use as key materials in nanodevice fabrication [1]. The research focus has been shifted from simple structures to a complex nanocrystal to achieve multifunctionality [2]. For that reason, hierarchically nanostructured materials are of great interest for field emission (FE)-based applications. Also, structures with nanotip emitters offer more excellent advantages than the usual microtip emitters. The small radius of curvature at the tip with a high aspect ratio facilitates the use of these field nanoemitters under lower applied voltages with a higher base pressure. The hierarchically nanostructured nanomaterials are attractive candidates for potential applications in a various range of vacuum micro/nanoelectronic devices. Nevertheless, to develop a simple, economically feasible and scaled-up method for constructing hierarchically self-assembled architectures is a daunting task for various systems.

In this regard, a promising methodology would be a solvothermal or hydrothermal approach [3]. Since, nano-Bi₂S₃ has intrinsic photoconductivity and, hence, has been explored for photo-enhanced FE behavior. The nanostructured Bi₂S₃ has been studied for field emission properties [4]. As seen from the literature, there are only a few reports on the FE characteristics of Bi₂S₃ nanostructures [5]. To improve the turn-on and threshold potential in Bi₂S₃ nanomaterials, the heterostructure architecture

has been used. More et al. [5] have reported the FE properties of the CdS-Bi₂S₃ heterostructure, which show the turn-on field is about 1.8 μV⁻¹ for 10 μA/cm².

In this paper, we report the synthesis of architected SrS/Bi₂S₃ consisting of self-assembled nanorods within nanoflowers via template-free solvothermal routes. After the illumination of visible light, these synthesized SrS/Bi₂S₃ nanoflowers exhibit reproducible photosensitive FE behavior. We investigate the FE performance of a single isolated SrS/Bi₂S₃ nanoflower to explore its application in FE-based micro/nano-optoelectronic devices. To the best of our knowledge, this unique SrS/Bi₂S₃ composite for FE performance has been hitherto unattempted and, hence, studied in detail.

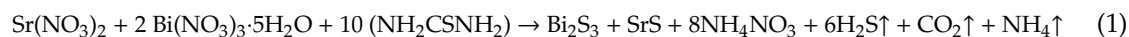
2. Materials and Methods

2.1. Material

Strontium nitrate (Sr(NO₃)₂), bismuth nitrate (Bi(NO₃)₃·5H₂O), and thiourea (NH₂CSNH₂-TU) are of analytical grade (SD Fine-Chem Limited, Mumbai, India) and were used for the synthesis of the catalyst without any further purification.

2.2. Synthesis of SrS/Bi₂S₃

In typical synthesis procedure, SrS/Bi₂S₃ nanostructures were prepared by dissolving 1 mmole of Sr(NO₃)₂, 2 mmole of Bi(NO₃)₃·5H₂O and 10 mmole of thiourea (NH₂CSNH₂) into 80 mL solvent (mixture of (3:1) water: ethylene glycol (EG)). After one hour of stirring, the solution was transferred to a Teflon-lined stainless steel autoclave (100 mL). Further, the system was sealed and kept at 180 °C in the oven, followed by natural cooling at room temperature. The finally obtained black precipitate was filtered, washed with water and ethanol 3–4 times, and dried at 80 °C. The samples were designated as S1, S2, and S3, which were synthesized in water: ethylene glycol (3:1) at 6 h, 12 h, and 18 h, respectively.



During reaction, ethylene glycol (EG): water was used as the reaction medium. Strontium nitrate, bismuth nitrate, and thiourea were dissolved in mixed solvent (EG and water) under magnetic stirring, then a clear yellowish solution was formed. In the solvothermal process, because of temperature and pressure, Bi₂S₃ and SrS nuclei were formed by the reaction of the Bi³⁺ and Sr²⁺ ions present in the solution and H₂S at solvothermal condition.

2.3. Sample Characterizations

The X-ray diffractometer (XRD, Model-D8, Advance, and Bruker AXS, Billerica, MA, USA) was used to investigate the structure. The FESEM (Hitachi S-4800, Tokyo, Japan) and transmission electron microscopy (TEM, JEM-2200FS, JEOL, Tokyo, Japan) were used to confirm the morphology and crystal size. Samples for TEM analysis were prepared by drop casting solutions onto carbon-coated copper grids followed by drying. The UV-Visible spectrometer (PerkinElmer Model-lambda-950, Rodgau, Germany) was used for optical study. The photoluminescence of the synthesized material was recorded on a Horiba Fluorolog-3 spectrofluorometer with an excitation wavelength of 420 nm. The variation in current was measured by an electrometer workstation (Keithley Electrometer, 6517B, Cleveland, OH, USA) with illumination of light (1500 LUX). We carried out Raman analysis for further investigation of the structural phases of the composite using a model HR-800-Raman spectrometer (Horiba JobinYvon, Paris, France 632).

2.4. Field Emission

The planar 'diode' configuration was used to measure field emission current density versus applied electric field (J–E), and emission current versus time (I–t) characteristics were measured in a metal vacuum chamber having a pressure of 1 × 10⁻⁸ mbar. A semi-transparent cathodoluminescent

phosphor screen (diameter ca. 50 mm) was kept parallel to the cathode in a typical ‘diode’ configuration. The cathode was obtained by sprinkling a very small quantity of the SrS/Bi₂S₃ powder onto a piece of conducting carbon tape (ca. 0.25 cm²), which was ultra-high vacuum (UHV) compatible. This carbon tape, along with the material, was further loaded on a copper rod connected to a linear motion drive, facilitating variation in the cathode–anode separation. During FE measurements, the cathode–anode separation was maintained at 2 mm constant distance. The emission current was acquired on a Keithley electrometer (6514) by varying the applied voltage between the cathode and anode with a step of 40 V (0–40 KV, Spellman, New York, NY, USA). The FE measurements and vacuum processing details were in accordance with the earlier reports [6]. For investigating the FE characteristics of a single isolated SrS/Bi₂S₃ nanoflower, a small quantity of the SrS/Bi₂S₃ powder was sonicated in acetone for 5 min and subsequently drop casted on a microscopic glass plate. Under a high-resolution optical microscope, a single SrS/Bi₂S₃ flower was skilfully picked up and carefully attached to a blunt tungsten tip using vacuum-compatible silver paste. The tungsten needle with a single flower was transferred to a stainless steel stub using UHV-compatible electrically conducting silver paint. A phosphor-coated tin-oxide concave glass plate (diameter ca. 50 mm) was used as an anode kept at a distance of ca. 3 cm, facing the sample (cathode).

3. Results and Discussions

3.1. Structural Study

The X-ray diffraction pattern of the urchin-like SrS/Bi₂S₃ nanostructure synthesized by varying reaction times is shown in Figure 1. The strong peaks can be assigned to the orthorhombic Bi₂S₃ (JCPDF card: 00-043-1471). The weak peaks at 29.68 and 42.42 are due to the cubic phase of the SrS (JCPDF card: 00-008-0489). The (111) indexed plane of SrS is merged in the (130) diffraction plane of Bi₂S₃. The intense and sharp peaks indicate that the urchin-like SrS/Bi₂S₃ nanostructure is well crystalline. The XRD shows that the obtained product is a composite, i.e., SrS/Bi₂S₃.

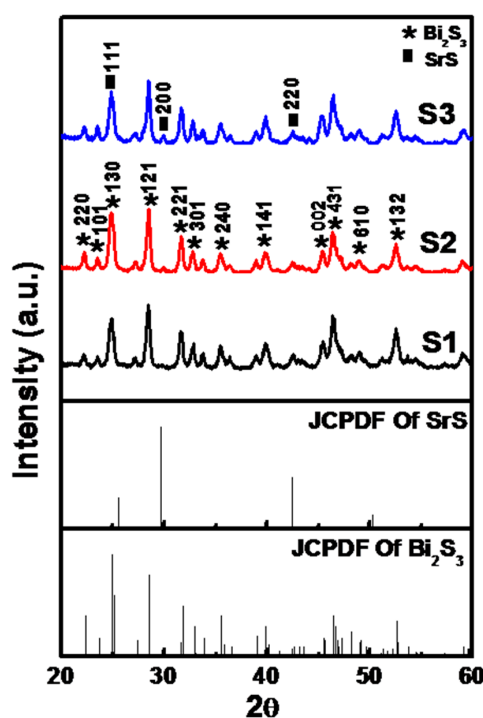


Figure 1. Pattern SrS/Bi₂S₃ nanoflowers synthesized by hydrothermal approach at 180 °C with different time durations: 6 h (S1), 12 h (S2), and 18 h (S3).

3.2. FESEM Study

Figure 2 shows typical FESEM micrographs of SrS/Bi₂S₃ synthesized at 180 °C for different reaction durations for morphological investigation. Figure 2a,b show the FESEM of sample S1, which shows the formation of a hierarchical flower-like structure containing nanorods with diameters of about 40 ± 5 nm, as well as hierarchical urchin-like micro-nanostructures having sizes of 3 ± 0.5 μm. Figure 2c,d are the images of sample S2 prepared at 12 h, which show uniform urchin-like micro-nanostructures having nanorods with lengths of 3.5 ± 0.5 μm and diameters of 40 ± 5 nm. When the reaction was prolonged to 18 h, urchin-like nanostructure flowers, as in Figure 2e,f, of size 4 ± 0.5 μm were formed by the self-alignment of nanorods of diameter 75 ± 5 nm. Phase formation of SrS took place in sample S3 and the intensity of peaks for SrS was increased in sample S3 than S2, which was observed in XRD and further confirmed via TEM. The flowers obtained are well defined and the self-alignment of nanorods is well separated, as compared to the S1 and S2 obtained within 6 h and 12 h. It is quite obvious to have bigger flowers with a higher diameter of nanorods because the crystal growth is favoured due to prolonged reaction time via the Ostwald ripening phenomenon [1].

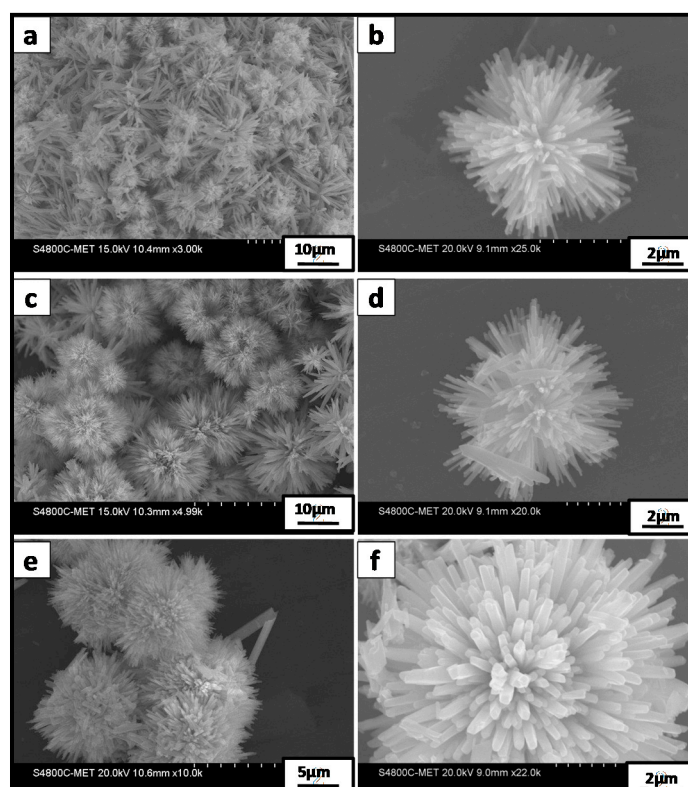


Figure 2. Images of the SrS/Bi₂S₃ synthesized by varying reaction times: S1 (a,b) for 6 h, S2 (c,d) for 12 h, and S3 (e,f) for 18 h.

3.3. HR-TEM Study

Figure 3 shows the high-resolution TEM (HR-TEM) images of an individual hierarchical SrS/Bi₂S₃ nanostructure with urchin-like morphology (sample S3). Figure 3a shows a characteristic TEM image of a SrS/Bi₂S₃ nanoflower composed of self-assembled nanorods. The HR-TEM of the sample S3 nanorod is shown in Figure 3b, having a rod size in the range of 50–80 nm. From the TEM images, the diameter of rods was observed to be consistent with FESEM investigations. Figure 3c, which shows the clear lattice fringes with d-spacing, reveals that the crystalline Bi₂S₃ nanoflower with lattice spacing of 0.31 nm, corresponding to the (121) plane (JCPDF card: 00-043-1471) of orthorhombic Bi₂S₃, is directly connected with the (200) plane (JCPDF card: 00-008-0489) of cubic SrS nanorods with lattice spacing of 0.30 nm. The selected area electron diffraction (SAED) pattern (Figure 3d) further confirms the

crystalline nature of the nanostructures and the calculated d-values are in good agreements with the XRD data. The uniform distribution of Sr and S Energy Dispersive X-Ray Analysis (EDAX) elemental mapping were performed, as shown in Figure 3e.

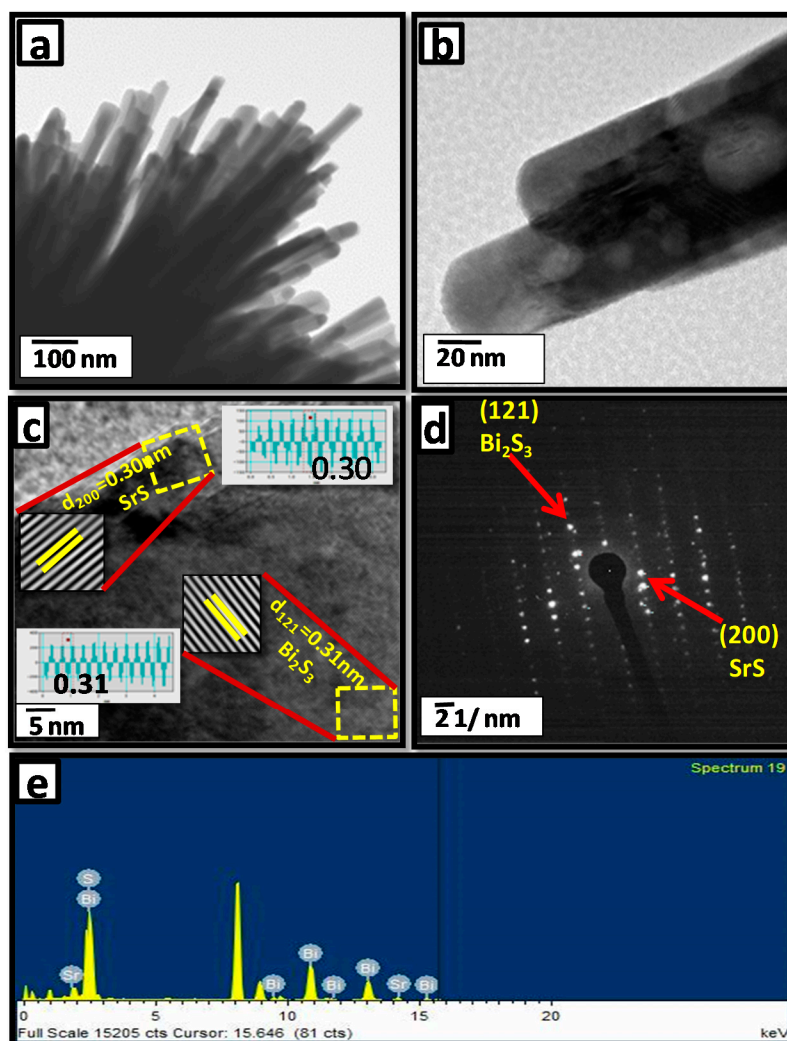


Figure 3. (a,b) TEM images of SrS/Bi₂S₃ nanoflower at different magnifications, (c) HR-TEM image of SrS/Bi₂S₃, (d) SAED pattern of corresponding SrS/Bi₂S₃ nanoflower, and (e) EDAX spectra of SrS/Bi₂S₃ nanoflower.

3.4. Optical and Electronic Studies

Figure 4 shows the ultra violet–visible (UV–VIS) absorption spectra of SrS/Bi₂S₃ samples. The absorption spectra were recorded over the wavelength range of 200–900 nm, implying that these samples may have good visible-light absorption. Interestingly, SrS content was not observed in sample S1 when the reaction was carried out for 6 h, which is also discussed in XRD. Samples S2 and S3 show identical absorption patterns with a steep absorption edge in the UV as well as visible region, corresponding to the band gap energy of the individual components. Amongst the various narrow band gap semiconductors, bismuth sulfide and strontium sulfide semiconductors have a direct band gap of ca. 1.3 eV and ca. 4.0 eV, respectively [7,8]. The band gap value was calculated using the Kubelka–Munk function $E_g = 1240/\lambda$ (where λ is the wavelength in nm) based on absorbance and was found to be two absorption steps at ca. 3.58 eV and ca. 1.64 eV corresponding to the SrS and Bi₂S₃, respectively, in sample S3. The absorption of this composite powder was shifted to shorter wavelengths monotonically as the SrS was added.

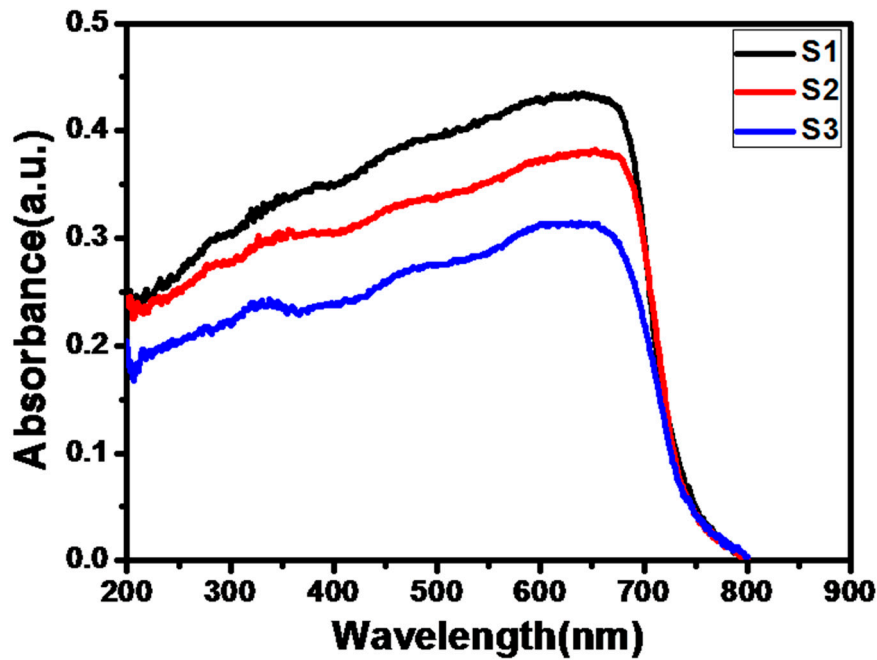


Figure 4. UV-Visible spectra of SrS/Bi₂S₃ synthesized by hydrothermal approach at 180 °C: S1, S2, and S3.

3.5. PL Study

Photoluminescence (PL) spectroscopy has been broadly used to study the efficiency of charge carrier trapping, movement, and the rate of recombination in semiconductors [1,9,10]. The room temperature photoluminescence (PL) measurement of prepared composite powders SrS/Bi₂S₃ was performed at 420 nm (Figure 5). The peak at 613 nm in the spectrum can be attributed to a high-level transition in SrS/Bi₂S₃ nanocrystallites [11]. However, the peak intensity in the case of sample S3 is less than S2 and S1. This may be an indication of Bi₂S₃ modification by SrS, which is getting adhered to the surface or within Bi₂S₃ bulk. These defects can act as the recombination centres for photo-generated carriers. The less electron-hole recombination in Bi₂S₃ resulted in the increase of PL peaks intensity [12]. The PL peaks intensities of the powders decreased from samples S1 to S3 with the phase formation of SrS. It indicates that the electron hole recombination is inhibited with increases in SrS.

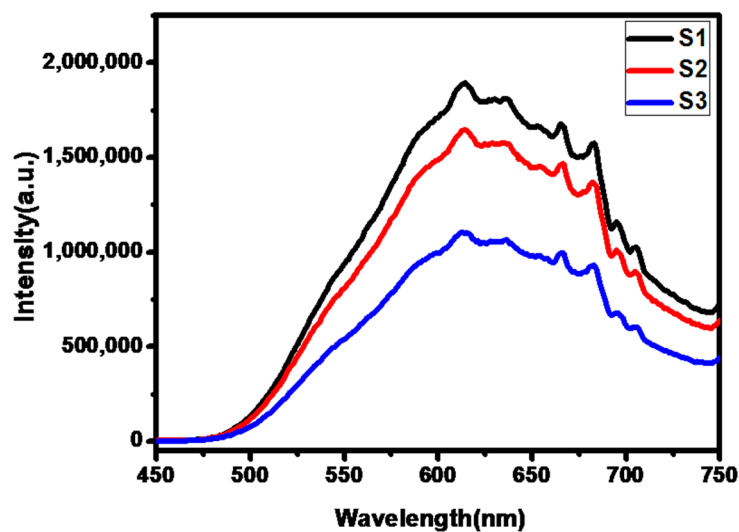


Figure 5. PL Spectra of the SrS/Bi₂S₃ samples S1, S2, and S3.

3.6. Raman Study

The room temperature Raman spectra of the SrS/Bi₂S₃ composite shown in Figure 6 and inset shows the Raman spectra of pure SrS. Raman spectroscopy is a vital tool for investigating the dopant concentration, identification of lattice defect, and orientation of crystals in the material [1]. Up to now, there was little work reported on the application of Raman spectroscopy on SrS nanostructures. The Raman spectrum exhibits four distinct vibrational peaks at about 78.78, 115.36, 245.55, and 964.47 cm⁻¹, which are assigned to Bi₂S₃. The two absorption bands at 78.78 and 115.36 are attributed to the Ag mode, while 245.55 cm⁻¹ is assigned to the B1g mode [13]. The peak at 965 cm⁻¹ may be to the surface phonon modes of nanosized Bi₂S₃ [3]. However, peaks at 451.41 cm⁻¹ and 615.12 cm⁻¹ are ascribed to SrS, which is slightly shifted due to composite structure (inset of Figure 6). Sample S3 has a little shift and the intensity is stronger than S1 and S2. According to Campbell [14], Raman scattering is considered to be very sensitive to the microstructures of nanocrystalline materials, which may lead to a shift, showing complete agreement with our results. The higher intensity of SrS/Bi₂S₃ composite (S3) in Raman was due to the good crystallinity of the material.

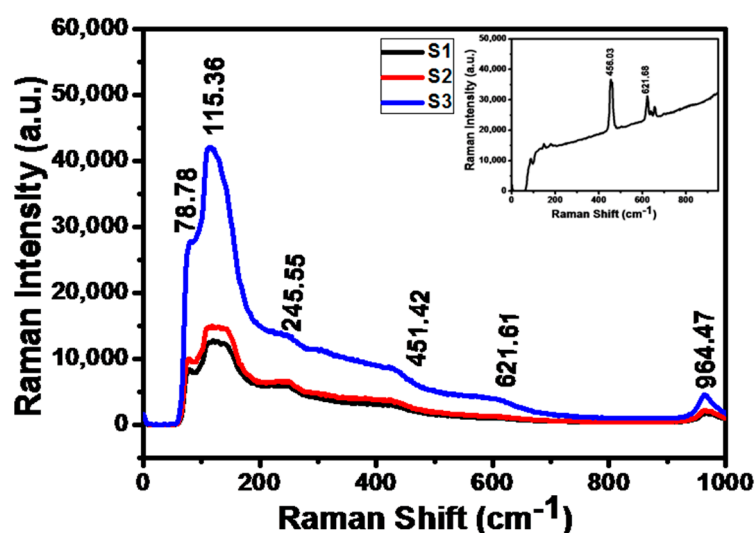


Figure 6. Raman Spectra of SrS/Bi₂S₃ nanoflowers and Inset show Raman spectra of commercial SrS.

4. Field Emission Study (FE)

The field emission current density J ($\mu\text{A}/\text{cm}^2$) versus applied field E ($\text{V}/\mu\text{m}$), i.e., J–E, characteristics of the SrS/Bi₂S₃ nanoflowers experiment was carried out in an UHV (Ultra High Vacuum) condition, at the base pressure of ca. 1×10^{-8} mbar and in a planar diode configuration. This is depicted in Figure 7 and Figure S1a,c,e (Supporting information). The J–E plot gives information about the turn-on field (defined as an applied field required to draw an emission current density of ca. $1 \mu\text{A}/\text{cm}^2$), the threshold field (defined as an applied field required to draw an emission current density of ca. $10 \mu\text{A}/\text{cm}^2$), and the maximum current density drawn [3,15]. The turn-on and threshold fields were found to be reproducible. The observed values of the turn-on field for Bi₂S₃, S1, S2, and S3 defined to draw an emission current density of ca. $1 \mu\text{A}/\text{cm}^2$ were found to be ca. 6.90, 2.55, and 2.50 V/ μm , and the threshold field to draw a current density of ca. $10 \mu\text{A}/\text{cm}^2$ was found to be ca. 7.40, 3.07, and 3.00 V/ μm (without visible light illumination) (Table 1). The size and shape of the emitter strongly affects FE behavior. Due to the high aspect ratio within nanomaterials, the nanostructure exhibits lower values of turn-on and threshold fields.

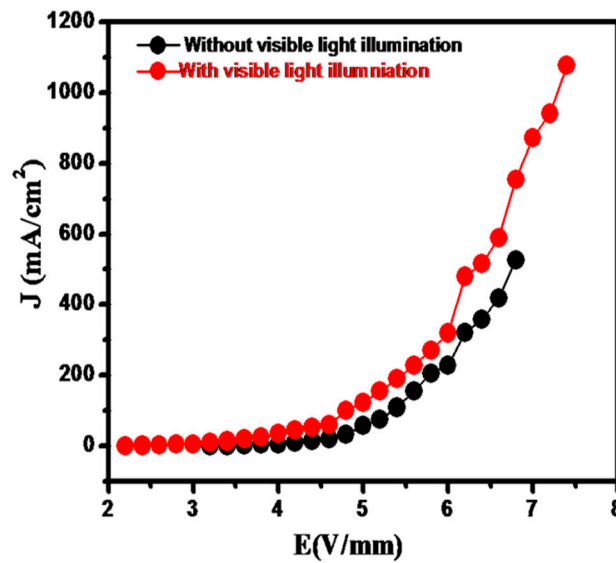


Figure 7. Emission current density–applied field (J–E) plot of the SrS/Bi₂S₃ (S3) nanoflowers.

Table 1. Emission study of SrS/Bi₂S₃ specimens.

| Specimen | Turn-on Field For 1 $\mu\text{A}/\text{cm}^2$ V/ μm Light Off/On | Threshold Field 10 $\mu\text{A}/\text{cm}^2$ V/ μm Light Off/On | Maximum Current Density $\mu\text{A}/\text{cm}^2$ Light Off/On |
|---|---|--|--|
| Bi ₂ S ₃ pristine | 3.10 | 3.84 | 60.32 |
| S1 | ca. 6.9/ca. 2.50 | ca. 7.4/ca. 3.20 | ca. 254/ca. 173 |
| S2 | ca. 2.55/ca. 2.37 | ca. 3.07/ca. 2.68 | ca. 264/ca. 284.8 |
| S3 | ca. 2.50/ca. 2.10 | ca. 3.00/ca. 2.80 | ca. 527/ca. 1078 |

Figure 7 shows an interesting enhancement in the field emission properties of SrS/Bi₂S₃ composites when photons of visible wavelength incident on the field emitter samples. It shows noticeable decrement in turn-on and threshold fields with visible light illumination [16]. With visible light illumination, the SrS/Bi₂S₃ emitter shows a turn-on field of ca. 2.50, 2.37, and 2.10 V/ μm and a threshold field of ca. 3.20, 2.68, and 2.80 V/ μm , respectively, for the anode–cathode separation of ca. 2 mm, which are very low values of the turn-on and threshold fields as compared to the values without visible light illumination. As the applied field increases gradually, the emission current density is observed to increase exponentially and a maximum emission current density of ca. 527, 264, and 254 $\mu\text{A}/\text{cm}^2$ is drawn at an applied field of ca. 7.4 V/ μm without light and a current density of ca. 1078, 284.8, and 173 $\mu\text{A}/\text{cm}^2$ at an applied field of ca. 6.9 V/ μm is observed as per the field emission theory. The observed J–E plots were analyzed using the Fowler–Nordheim (F–N) equation [17]. The result obtained is much superior to pristine Bi₂S₃ (Table 1). Figure 8 and Figure S1b,d,f in Supporting Information shows the corresponding F–N plot, i.e., plot of $\ln(J/E^2)$ versus $(1/E)$, (b, d, f) derived from the observed J–E characteristics. In both cases, the emitter has a semiconducting nature, which is confirmed over the entire range of the applied field in F–N plots with nonlinear behavior.

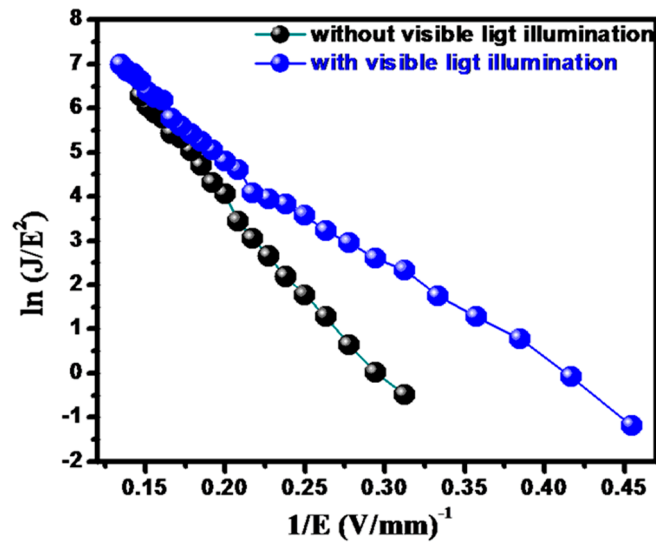


Figure 8. Fowler–Nordheim (F–N) plot of the SrS/Bi₂S₃ (S3) nanoflowers.

Interestingly, the F–N plot of the field emission current from the SrS/Bi₂S₃ displays a nonlinear relationship between $\ln(J/E^2)$ versus $1/E$ for both, without light and with light illumination. This nonlinearity can be explained by the non-uniform geometries of the emitters. The F–N plot shows a gradual bend in the curve for the low electric field and then much more steeper change is observed in the high field region [18,19]. The nonlinearity of the F–N plot is dominated by geometrical variations of the protrusions in the SrS/Bi₂S₃. With increasing applied voltage, the number of emission sites increases, ultimately resulting in a rising slope as a function of the electric field. The linear behavior of the F–N curve was observed only at the highest electric field. Along with the emission characteristics, the emission current stability of the field emitters is an essential parameter in the context of their practical application. The emission current stability has been investigated at the base pressure of ca. 1×10^{-8} mbar.

The emission current versus time (I–t) measurement of sample S3 was performed at a preset current value of ca. 10 μ A over the period of 3 h and long-term stability over the period of 10 h was found to be fairly stable with 13.2 ± 10 mA current (Figure 9a,b). The appearance of spikes in the emission current is endorsed for the adsorption, desorption, and migration of residual gas molecules on the emitter surface.

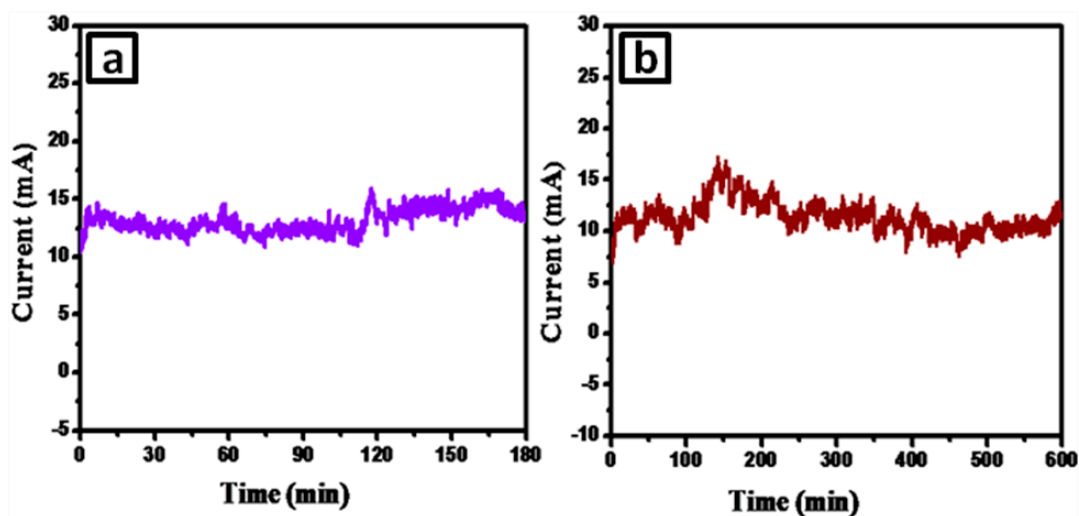


Figure 9. Emission current versus time (I–t) plots of the SrS/Bi₂S₃ (S3) nanoflowers (a,b).

A field emission micrograph for sample S3 captured at the different applied fields shows a current density of ca. $400 \mu\text{A}/\text{cm}^2$ and displays a number of tiny bright spots (Figure 10), indicating that the emission is indeed from protruding emitting sites [20]. The temporal changes in the intensity of these spots are observed to be commensurate with the emission current fluctuation, depicted in the I–t plot (Figure 11).

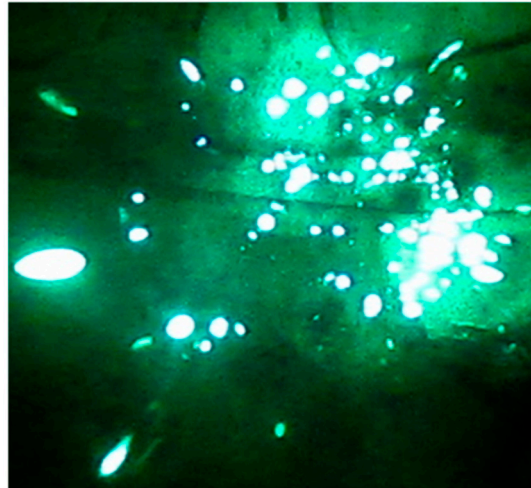


Figure 10. Field Emission Micrograph (FEM) image of SrS/Bi₂S₃ (S3).

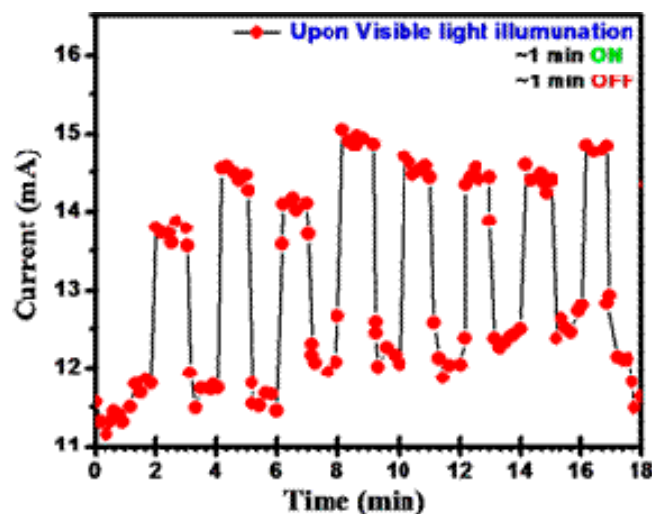


Figure 11. FE behavior of the SrS/Bi₂S₃ (S3) nanoflowers.

Based on previous reports [21], we proposed a mechanism of field emission enhancement in 3D SrS/Bi₂S₃ nanoflowers due to hierarchical architectures. The heteroarchitected SrS/Bi₂S₃ (S3) emitter exhibits superior emission behavior, which can be attributed to the combined effect. The unique morphological patterns of the SrS/Bi₂S₃ emitter are responsible for field emission enhancement. The epitaxial growth of SrS on the Bi₂S₃ nanorods (stem) is an important player in enhancing the ‘local’ field of the SrS/Bi₂S₃ emitter. In this ‘two-stage’ process, the ‘first’ enhancement in the local field was due to the ‘Bi₂S₃’ stem and further enhancement at the ‘branches’ (SrS) was owing to their high aspect ratio [22]. This is confirmed from PL results, which indicate that defects provided the recombination centers for photo-generated carriers, and less electron-hole recombination in SrS/Bi₂S₃. The PL peaks intensities of the powders decreased from samples S1 to S3 with the phase formation of SrS. It indicates that the electron hole recombination is inhibited with the increase in SrS. The defect vacancies further lead to a lowering of the surface barrier, which in turn is expected to increase the carrier mobility and

conductivity [23]. Such surface passivation effects are observed in the SrS/Bi₂S₃ nanoflower, which is responsible for better FE.

5. Conclusions

In a nutshell, nanoflowers of strontium sulfide/bismuth sulfide were synthesized by the hydrothermal method. The effect on the morphologies and size of SrS/Bi₂S₃ were studied with respect to the reaction time. This structural study shows the orthorhombic and cubic phases of Bi₂S₃ and SrS, respectively. The flowers of micron size were comprised of nanorods with a size of 50–80 nm. Considering the tunable band gap of these nanostructures within the visible region, field emission investigation was demonstrated. The turn-on and threshold fields were found to be reproducible, with ca. 1 $\mu\text{A}/\text{cm}^2$ found to be ca. 2.5 V/ μm and ca. 10 $\mu\text{A}/\text{cm}^2$ found to be ca. 3.00 V/ μm (without visible light illumination), respectively. This composite (S3) shows an interesting enhancement in the field emission properties of SrS/Bi₂S₃ when photons of visible wavelength incident on the field emitter. With visible light illumination, the SrS/Bi₂S₃ emitter shows a turn-on field of ca. 2.50 V/ μm and a threshold field of ca. 2.80 V/ μm , respectively, for an anode–cathode separation of ca. 2 mm. These values of the turn-on and threshold fields are lower as compared to the values obtained without visible light illumination. The SrS/Bi₂S₃ is a promising candidate for microelectronics applications.

Supplementary Materials: The following are available online at <http://www.mdpi.com/2504-477X/3/4/105/s1>, Figure S1: J-E and Current versus time (I–t) plots for S1 (a,b) (6 hr), S2 (c,d) (12 hr) and (e,f) Pristine Bi₂S₃.

Author Contributions: A.R.G.: Methodology, Investigation, Writing-Original Draft Preparation. U.P.C. and Y.A.S.: Software, Writing-Review & Editing, Visualization. R.P.P. and J.D.A., M.A.M.: Formal Analysis. M.V.K. and B.B.K.: Conceptualization, Supervision.

Funding: This research received no external funding.

Acknowledgments: The authors would like to give thanks for the Ministry of Electronics and Information Technology (MeitY) Government of India and Centre for Materials for Electronics Technology (C-MET), Pune for providing research facilities. The authors would like to thank Nanocrystalline materials group for their kind support.

Conflicts of Interest: The authors declare no conflict of interest.

References

1. Yu, X.; Cao, C. Photoresponse and Field-Emission Properties of Bismuth Sulfide Nanoflowers. *Cryst. Growth Des.* **2008**, *8*, 3951. [[CrossRef](#)]
2. Zhai, T.L.; Ma, L.Y.; Liao, M.; Wang, X.; Fang, X.; Yao, J.; Bando, Y.; Golberg, D. One-dimensional inorganic nanostructures: Synthesis, field-emission and photodetection. *Chem. Soc. Rev.* **2011**, *40*, 2986. [[CrossRef](#)] [[PubMed](#)]
3. Panmand, R.P.; Sethi, Y.A.; Deokar, R.S.; Late, D.J.; Gholap, H.M.; Baeg, J.; Kale, B.B. In situ fabrication of highly crystalline CdS decorated Bi₂S₃ nanowires (nano-heterostructure) for visible light photocatalyst application. *RSC Adv.* **2016**, *6*, 23508–23517. [[CrossRef](#)]
4. Yu, Y.; Jin, C.H.; Wang, R.H.; Chen, Q.; Peng, L.-M. High-Quality Ultralong Bi₂S₃ Nanowires: Structure, Growth, and Properties. *J. Phys. Chem. B* **2005**, *109*, 18772–18776. [[CrossRef](#)] [[PubMed](#)]
5. Warule, S.S.; Kashid, R.V.; Shinde, D.R.; Chaudhari, N.S.; Kale, B.B.; More, M.A. Architected Bi₂S₃ nanoflowers: Photoenhanced field emission study. *J. Nanopart Res.* **2012**, *14*, 889. [[CrossRef](#)]
6. Ibanez, M.; Guardia, P.; Shavel, A.; Cadavid, D.; Arbiol, J.; Morante, J.; Cabot, A. Growth Kinetics of Asymmetric Bi₂S₃ Nanocrystals: Size Distribution Focusing in Nanorods. *Phys. Chem. C* **2011**, *115*, 7947. [[CrossRef](#)]
7. Ramgir, N.S.; Late, D.J.; Bhise, A.B.; Mulla, I.S.; More, M.A.; Joag, D.S.; Pillai, V.K. Field emission studies of novel ZnO nanostructures in high and low field regions. *Nanotechnology* **2006**, *17*, 2730. [[CrossRef](#)]
8. Khan, Z.; Barpuzary, D.; Baswant, O.; Sutradhar, S.; Qureshi, M. Directed growth of 1D cadmium sulfide by chemically anchored Al₂O₃ and ZnO (nanoparticles). *Mater. Lett.* **2011**, *65*, 1168. [[CrossRef](#)]
9. Li, F.B.; Li, X.Z. The enhancement of photodegradation efficiency using Pt-TiO₂ catalyst. *Chemosphere* **2002**, *48*, 1103. [[CrossRef](#)]

10. Zhang, J.; Hu, Y.; Matsuoka, M.; Yamashita, H.; Minagawa, M.; Hidaka, H. Relationship between the Local Structures of Titanium Oxide Photocatalysts and Their Reactivities in the Decomposition of NO. *J. Phys. Chem. B* **2001**, *105*, 8395. [[CrossRef](#)]
11. Cong, Y.; Zhang, J.; Chen, F.; Anpo, M.; He, D. Preparation, Photocatalytic Activity, and Mechanism of Nano-TiO₂ Co-Doped with Nitrogen and Iron (III). *J. Phys. Chem. C* **2007**, *111*, 10618. [[CrossRef](#)]
12. Niasaria, M.S.; Ghanbaria, D.; Davara, F. Synthesis of different morphologies of bismuth sulfide nanostructures via hydrothermal process in the presence of thioglycolic acid. *J. Alloys Compd.* **2009**, *488*, 442. [[CrossRef](#)]
13. Wang, Y.; Chen, J.; Jiang, L.; Sun, K.; Liu, F.; Lai, Y. Photoelectrochemical properties of Bi₂S₃ thin films deposited by successive ionic layer adsorption and reaction (SILAR) method. *J. Alloys Compd.* **2016**.
14. Campbell, I.H.; Fauchet, P.M. The effects of microcrystal size and shape on the one phonon Raman spectra of crystalline semiconductors. *Sol. State Commun.* **1986**, *58*, 739. [[CrossRef](#)]
15. Liu, Z.; Huang, W.; Zhang, Y.; Tong, Y. Facile hydrothermal synthesis of Bi₂S₃ spheres and CuS/Bi₂S₃ composites nanostructures with enhanced visible-light photocatalytic performances. *CrystEngComm* **2014**, *12*, 8261. [[CrossRef](#)]
16. Kar, S.; Chaudhuri, S.C.J. Shape Selective Growth of CdS One-Dimensional Nanostructures by a Thermal Evaporation Process. *J. Phys. Chem. B* **2006**, *110*, 4542. [[CrossRef](#)]
17. Warule, S.S.; Chaudhari, N.S.; Kale, B.B.; Pandiraj, S.; Khare, R.T.; More, M.A. Controlled synthesis of aligned Bi₂S₃ nanowires, sharp apex nanowires and nanobelts with its morphology dependent field emission investigations. *CrystEngComm* **2013**, *15*, 890. [[CrossRef](#)]
18. Fowler, R.H.; Nordheim, L.W.; Proc, R. Electron emission in intense electric fields. London. *Ser. A* **1928**, *119*, 173. [[CrossRef](#)]
19. Palnitkar, U.A.; Kashid, R.V.; More, M.A.; Joag, D.S.; Panchakarla, L.S.; Rao, C.N.R. Remarkably low turn-on field emission in undoped, nitrogen-doped, and boron-doped graphene. *Appl. Phys. Lett.* **2010**, *97*, 063102. [[CrossRef](#)]
20. Chavan, P.G.; Badadhe, S.S.; Mulla, I.S.; More, M.A.; Joag, D.S. Synthesis of single crystalline CdS nanocombs and their application in photo-sensitive field emission switches. *Nanoscale* **2011**, *3*, 1078–1083. [[CrossRef](#)]
21. Bankar, P.K.; Pawar, M.S.; Pawbake, A.S.; Warule, S.S.; Late, D.J.; More, M.A. Spatially branched CdS–Bi₂S₃ heteroarchitecture: Single step hydrothermal synthesis approach with enhanced field emission performance and highly responsive broadband photodetection. *RSC Adv.* **2016**, *6*, 95092–95100. [[CrossRef](#)]
22. Zhirnov, V.V.; Givargizov, E.I.; Plekhanov, P.S. Field emission from silicon spikes with diamond coatings. *J. Vac. Sci. Technol.* **1995**, *13*, 418–421. [[CrossRef](#)]
23. Warule, S.S.; Chaudhari, N.S.; Kale, B.B.; Patil, K.R.; Koinkar, P.M.; More, M.A.; Murakami, R.-I. Organization of cubic CeO₂ nanoparticles on the edges of self assembled tapered ZnO nanorods via a template free one-pot synthesis: Significant cathodoluminescence and field emission properties. *J. Mater. Chem.* **2012**, *22*, 8887–8895. [[CrossRef](#)]

